ELSEVIER

Mesoscale design of multifunctional 3D graphene networks

Peter C. Sherrell and Cecilia Mattevi*

Department of Materials, Royal School of Mines, Imperial College London, London SW7 2AZ, United Kingdom

Three-dimensional graphene networks are emerging as a new class of multifunctional constructs with a wide range of potential applications from energy storage to bioelectronics. Their multifunctional characteristics stem from the unique combination of mechanical properties, electrical conductivity, ultra-low density, and high specific surface areas which distinguish them from any polymer, ceramic or metal constructs. The most pressing challenge now is the achievement of ordered structures relying on processes that are highly controllable. Recent progresses in materials templating techniques, including the advent of three-dimensional printing, have accelerated the development of macroscopic architectures with micro-level-controlled features by rational design, with potential for manufacturing.

Introduction

Graphene presents a unique combination of exceptional properties, encompassing optical transparency, ultra-high surface area, high mechanical strength, and high carrier mobility [1,2]. These properties have inspired the creation of macroscopic self-supporting three-dimensional counterparts of graphene which can present multifunctional characteristics.

To this end, the last few years have seen a steadily increasing number of publications on the fabrication of graphene three-dimensional (3D) complex structures. The most sought properties of the networks encompass ultralow density, high surface area, high mechanical strength, electrical conductivity, and optical transparency, as they can enable diverse potential applications such as: energy storage and energy conversion devices [3–6], environmental systems [7], bioelectronics [8–11], oil sorption and filtration [7,12,13]. The expectation for 3D structure is to exhibit properties arising from the synergistic combination of the graphene characteristics and the specific architectural assembly. The most pressing challenge in making 3D structures suitable for applications is twofold; the achievement of coherent, tailorable, and predictable graphene architectures by manipulating the processing parameters, and understanding the correlation between ordering and properties. Similar challenges have been recognized for decades in the area of metal and ceramic foams [14].

In this review we will provide an overview of the different structuring methods proposed so far and we will present them in the context of the present challenge, analyzing the microstructural ordering and related properties. The two methodologies adopted to build these networks are either based on solution processing techniques or chemical vapor deposition (CVD). The former uses graphene oxide (GO), as a precursor to graphene, and is based on processes well established for polymers and ceramic materials [12,15], involving few fabrication steps, and is potentially scalable. While the second approach, based on the CVD synthesis of pristine graphene [16–22] adapted to a 3D geometry, yields higher electrical conductivity in the network yet involves multiple fabrication steps. We highlight the impact of processing parameter control on the microstructure, and subsequently, physical and electrical properties of the resulting macroscopic 3D graphene architectures. The first part of this review delves into solution processing based strategies whilst the second focuses on CVD synthesized architectures.

Liquid phase processing

Chemically modified graphene

Graphene oxide, since its advent, has been proposed as a building block for mechanically very strong constructs with

**Corresponding author:* Mattevi, C. (c.mattevi@imperial.ac.uk)

 http://dx.doi.org/10.1016/j.mattod.2015.12.004

Please cite this article in press as: P.C. Sherrell, C. Mattevi, Mater. Today (2016), http://dx.doi.org/10.1016/j.mattod.2015.12.004

multifunctional properties [23]. First studies have shown the formation of robust paper materials along with the assembly of new conductive polymeric and ceramic composites with GO flakes [24]. GO is a chemical derivative of graphene where oxygen functional groups (hydroxyl and epoxy group on the basal plane and carboxyl and hydroxyl at the edges of the flakes) are covalently bound to the carbon atoms of the honeycomb structure (Fig. 1a) [23]. The ionic nature of most of the functional groups, which allows protonation or deprotonation in water, is a useful tool to control assembly, disassembly, and stability of the GO sheets in solution. Deprotonation of these species in water leads to electrostatic repulsion between GO flakes, facilitating the formation of colloidal suspensions.

GO can be easily obtained by a scalable process of oxidation of commercially available graphite powers [25,26] with the lateral size of monolayers typically being in the range of 10–50 μm which can be reduced to a few microns by ultrasonication in aqueous suspension [27]. Owing to this range of characteristics, GO can be processed as either a microparticle or a macromolecule, allowing us to adopt processing methods of both ceramic particles and polymers.

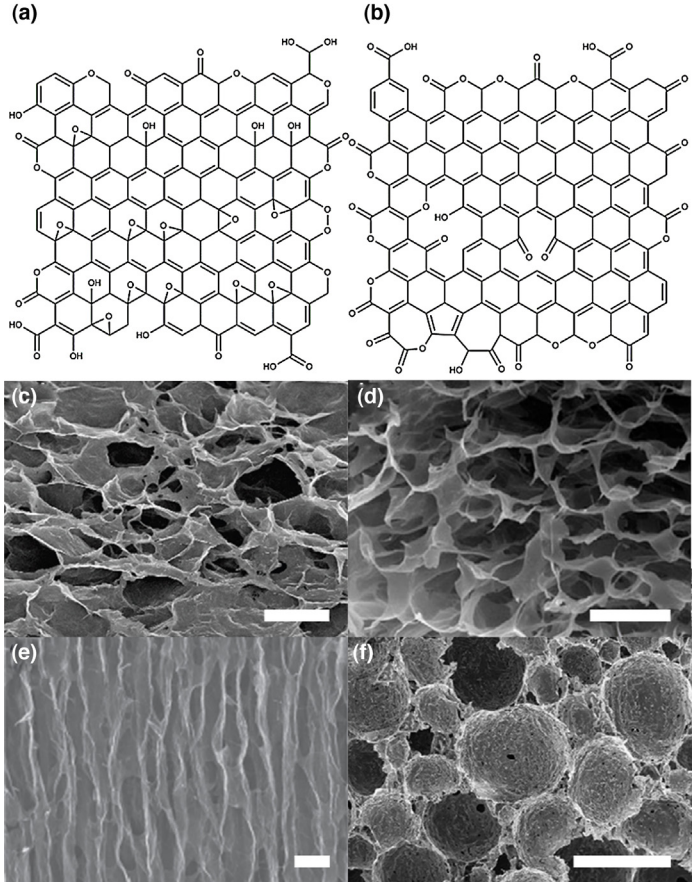

FIGURE 1

Chemical structure of: (a) graphene oxide; (b) chemically modified graphene. Scanning electron micrographs (SEMs) of: (c) CMG network from self-assembly, scale bar 5 μm (reproduced with permission from [15]); (d) CMG network from sol–gel processing, scale bar 5 μm (reproduced with permission from [47]); (e) CMG with lamellar structure from freeze-casting, scale bar 50 μm (reproduced with permission from [60]); and (f) CMG with a cellular structure from freeze-drying, scale bar 100 μm (reproduced with permission from [12]).

In addition, upon heating and/or exposure to reducing agents [23,28,29], electrical conductivity can be partially restored due to the loss of oxygen functionalities leaving a partially reconstructed hexagonal sp^2 carbon lattice (Fig. 1b) [12]. The resulting material is often named chemically modified graphene (CMG) or reduced GO.

Gelation of chemically modified graphene

The assembly of GO flakes was initially inspired by polymer processing to obtain hydrogels and aerogels. Observations that GO flakes spontaneously self-assemble upon chemical reduction in water reaching a gelation point led to the realization of the first graphene based-hydrogels [15]. Reduction and gelation of GO occurs in aqueous environment (or alcohol [30]) by applying mild heating (95–180°C) [7,15,31,32] to a GO suspension in an autoclave or, alternatively, at atmospheric pressure with the possible addition of reducing agents (L-ascorbic acid, ammonia, $NaHSO_3$, Na_2S, HI hydroquinone) [7,33–38]. The coagulation is promoted by the loss of ionic oxygen functionalities and the subsequent attractive van der Waals forces and hydrogen bonding between the sheet basal planes [39]. Coagulation in a still suspension ultimately leads to the formation of a reticulated 3D structure of CMG sheets. The remaining oxygen content varies depending on the temperature applied, normally within the range of 10–15 at.% [15,33,36,37] with few exceptions at lower percentages [38] when post thermal treatment at temperature higher than 900°C are applied. The obtained structures are self-supporting hydrogel monoliths, mechanically robust, and ultra-lightweight.

The microstructure of these hydrogels/aerogels appears as a random network of wrinkled CMG walls, filamentary strands and pores, which loosely resemble a cellular shape (Fig. 1c). From metals and ceramics materials, it is known that highly regular isotropic structures with high connectivity from the nonmetric to micrometric scale can yield high Young's modulus [14]. Structures with such characteristics can have Young's modulus linearly dependent to the mass density which is desirable to be able to lower their weight preserving the stiffness, on the contrary of materials with random porosity that exhibit a cubic dependence with the mass density [14]. Ultimately it is desirable to have ultralow density graphene networks with high stiffness and to this we need to design hierarchical architecture from the nano- to the microscale with wall/struts characteristics and isotropic geometry.

The mass densities reported are in the range between 0.16 mg/cm^3 [13,30] and 1600 mg/cm^3 [33,36–38,40,41] comparable to polymer or carbon nanotubes aerogels and the monoliths can demonstrate elastic and elastic–plastic [15] mechanical behavior. Investigation of the specific Young's modulus has revealed values from 0.1 MPa to 6.2 MPa [15,33,36,37] as well as yield stress values from 3 kPa to 28 kPa [15,33,36,40]. Considering the density of these materials is in the range of tens of mg/cm^3, the Young modulus is remarkable and overall superior to CNT sponges [42,43] and metallic microlattices [44] of comparable mass density [14,33].

These structures present meso-porosity to macro-porosity that invariably contributes to increase the Brunauer–Emmett–Teller (BET) specific surface area reported in the range 11–500 m^2/g [7,36] where the lowest surface area has been reported for highly restacked-paper like CMG.

Please cite this article in press as: P.C. Sherrell, C. Mattevi, Mater. Today (2016), http://dx.doi.org/10.1016/j.mattod.2015.12.004

The electrical conductivity values present a wide range of variability, reflecting microstructural differences (Fig. 2).

The final shape of the structures is conformal to the gelation vessel providing a method to generate monolithic foams in conformable shapes. Residual water retained by the hydrogels can lead to structural instability thus such hydrogels are dried to aerogels. This drying process has to be carefully designed to avoid the collapse of the flexible walls of the structure under the capillary forces exerted by the residual absorbed water. To this end, supercritical CO_2 drying [33] or freeze-drying [33] is the processing methods of choice to replace water with air to obtain a mechanically stable aerogels, with CO_2 super critical drying producing more stable and higher surface area structures [36]. The final aerogels retain similar microstructures to the starting hydrogels while demonstrating increased mechanical and thermal stability [33].

Self-assembly of CMG through gelation is useful due to the ease of processability, however, it offers low control over the final microstructure. This lack of controllability is in part due to the lack of standardization of GO processing (from synthesis parameters, purification protocols, and flake lateral size) and in part the lack of systematic and comprehensive studies aiming to correlate processing parameters (GO concentration, aging time, gelation time, drying process) and microstructural characteristics. A certain degree of control over pore size (between 2 μm and 6 mm) has been achieved by controlling the initial concentration of the GO suspensions (between 0.6 mg/mL and 2 mg/mL) and/or reaction time [15,31,33,36], while selecting only flakes with lateral size in tens of microns [30] has led to monoliths with super compressive elasticity. In addition, changing the pH of the GO suspension has led to controlling the final density of the monolith and ultimately their mechanical and electrical properties [38], although microstructural changes have been not identified [38].

Concurrently, a chemical cross linking route to synthesize CMG aerogels has been proposed in an attempt to increase the electrical conductivity, surface area, and density of the aerogels [45,46]. To this end, sol–gel based strategies as well as the use of polymeric

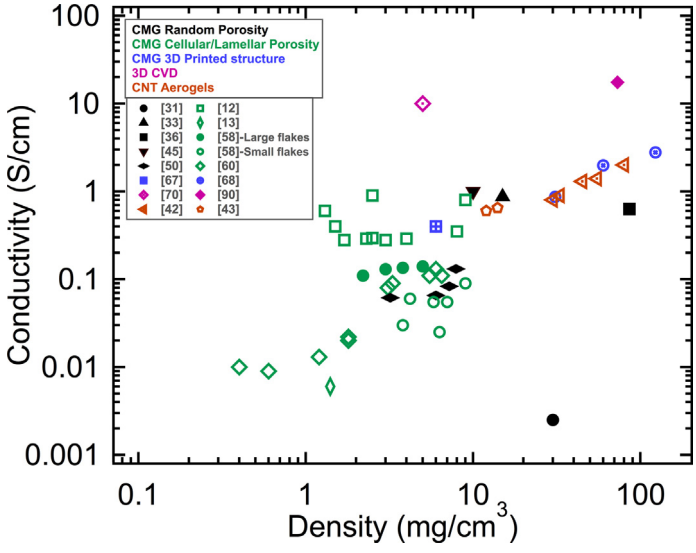

FIGURE 2

Electrical conductivity versus mass density of the monoliths of both solution processed CMG networks and CVD 3D graphene networks, highlighting differences with production techniques.

cross-linking between the hydroxyls group in GO have been explored. Sol–gel chemistry based on carbon-reticulating agents has been applied to colloidal suspensions of GO [36,45–47] in a similar way to previous studies toward reticulating carbon nanotubes [42]. The sol–gel technique is a widely used wet-chemistry technique for the fabrication of ceramic materials through a polymerization process occurring at close to room temperature [48].

The first process proposed to cross link GO flakes involves resorcinol and formaldehyde and sodium carbonate as a catalyst which are mixed in an aqueous suspension of GO sealed in glass vials at 85°C [45]. GO-RF gels are subsequently dried and pyrolysis (1050°C) under inert atmosphere which yields a graphene aerogel [45]. Different variations of chemical reagents have been proposed since, along with the addition of polymers to promote cross linking (resol-type phenolic pre-polymers) [47,49–51].

CMG monoliths present microstructures comparable to reduction-based approaches, with an entanglement of filamentary flakes, wrinkled walls, and random porosity (Fig. 1d) with a low density (7.9 mg/cm^3 [50], 10 mg/cm^3 [45], 16 mg/cm^3 [49], and 20 mg/cm^3 [47]) and a high surface area (1019 m^2/g [50], 584 m^2/g [45], 1199 m^2/g [49], 700 m^2/g [47]).

While the mechanical properties of these constructs have been barley explored, overall the reported electrical conductivity [49,50] is slightly greater than the physically-assembled structures of comparable density (Fig. 2). This could suggest an increased connectivity between flakes toward a thoroughly 3D 'struts and walls' network and further investigation of sol–gel processing could elucidate on this aspect.

We can therefore conclude that physical and covalent assembly methods are easy to implement, but present very low control of processing parameters and very low degree of microstructural ordering. Further added value can be induced through the incorporation of different nanomaterials, such as metal, metal oxide nanoparticles, and other 2D materials [52], at any stage of the structure fabrication, where such combinations demonstrate promise for a diverse range of applications, including energy storage, catalysis, and sensing. However, further work would be necessary to understand the correlation between processing parameter and final characteristics of the monoliths to be able to engineer any practical application.

It is worth noting that highly porous monoliths of semiconducting direct band gap 2D materials (MoS_2, WS_2) have recently appeared, suggesting a new surging wave of graphene analogs networks [53].

Soft and hard sacrificial templates: cellular and lamellar graphene networks

Solution based templating techniques typically utilized for ceramic materials, such as unidirectional freeze casting [54,55], and emulsification [56], can offer a high degree of control over processing parameters. These methods are known for their ability to provide lamellar and cellular networks of ceramic materials respectively. During unidirectional freezing, segregation between ice formation and solid particles occurs and, in steady state conditions, ice can grow as anisotropic crystals widely elongated along the temperature gradient direction resulting in solid particles segregated between adjacent ice lamellae. Subsequent replacement of the liquid phase with air under a sublimation process

Please cite this article in press as: P.C. Sherrell, C. Mattevi, Mater. Today (2016), http://dx.doi.org/10.1016/j.mattod.2015.12.004

(freeze drying conditions) will leave a porous lamellae structure. Emulsion templating can generate cellular porosity if amphiphilic solid particles are confined at the interface between two immiscible liquids, like oil in water emulsions. Since GO can stabilize Pickering emulsions [57] due to its amphiphilic nature, emulsion templating can be employed for GO. Low pH will favor self-assembly of the flakes at the oil water interfaces [57], driven by van der Waals and hydrogen bonding forces. The final microstructure will therefore present a cellular porosity (Fig. 1d) where the walls are formed by several GO flakes assembled face-to-face with a thickness that can be tuned by the initial GO concentration and pH [12,57]. Depending of the presence of different additives it is also possible to form either open cell porosity or closed cell porosity [12].

Unidirectional freeze-casting of GO [12,58,59] or of CMG water suspensions [60–62] yields free-standing structures with lamellar porosity [58,60] (Fig. 1e) where the walls are formed by self-assembled GO/CMG layers. The thickness of the walls and thus the width of the porous channels and their shape can be reliably controlled by the speed of the freezing front [58,60,61] and GO/CMG concentrations [12,58]. The addition of polymer binders (such as PVA [12] or Nafion [59]) or the organic phase in emulsions, can affect the microstructures in multiple ways, from the pore size to their interconnectivity [12] (Fig. 1f). The combination of the two methods, through unidirectional freezing of GO emulsions, provides a further degree of tunable cell porosity producing elongated polyhedrons [12,58]. The manipulation of these process parameters provides precise and predictable changes in the microstructure of the network. CMG monoliths can be then annealed at high temperatures (700–2400 K) [12,58,60,61] to render them mechanically stable and electrically conductive. Mechanical properties can be highly tunable from superelastic [58,60] to elastic brittle behavior [12].

The mechanical response appears to be mostly affected by the walls crystallinity and thickness rather than the microstructure connectivity [58]. However, further understanding will be needed to clarify the interplay between walls characteristics and pore architecture to determining the physical response. What is worth noting is that ultra-light networks with thick walls formed by stacking of several graphene layers present superior mechanical properties than networks of the same density formed with smaller-sized pores and therefore with thinner graphene walls [58]. This emphasizes how the van der Waals interaction between graphene sheets determines the overall strength of the monolith. In addition the mechanical properties improve with annealing temperature, which reduces the oxygen functionalities and heals crystallographic defects [12,58,60,61]. It is therefore apparent that structures resembling a pristine graphene network exhibit enhanced robustness and elasticity. Not surprisingly, these characteristics also increase the electrical conductivity (Fig. 2), as reported networks annealed at very high temperatures, such as 2400°C [12], present the highest electrical conductivity compared to networks of similar density. This is only lower than the CVD graphene-based networks. In addition, irrespective of the assembly method and final microstructure the electrical conductivity is higher for networks which have been annealed at temperatures greater than 1000°C [12,45,58] and concurrently are formed by flakes with lateral size of a few tens of microns versus networks formed by flakes smaller than 2 μm [30,58] (Fig. 2).

Indeed, another characteristic that is critical for any structuring method is the lateral size of the GO/CMG flakes. There is evidence that GO flakes with lateral size distribution centered at 25 μm [30,58] can yield a very ordered lamellar microstructure. While GO flakes with lateral size distribution centered at 2 μm do not generate a well-defined ordered structure, presenting random porosity. Such structures then exhibit mechanical and electrical properties of approximately one order of magnitude lower than analogous samples made with larger GO flakes [30,58]. This variance emphasizes how the flakes lateral size and thus the extension of the van der Waals forces plays a key role in the assembly process, and better understanding of this parameter would greatly accelerate research progress in this and several other technology areas. The CMG aerogels with periodic order (lamellar of cellular porosity or in between) [12] present reversible deformation and tunability between elastic-brittle to elastomeric behavior with a macroscopic elastic response [60] (Fig. 3a).

The actual Young's modulus is either comparable (0.1–50 kPa at 0.2–8 mg/cm^3 density) [60] or superior (20–800 kPa at densities 2–10 mg/cm^3 for lamellar porosity [58] and between 10 and 10 MPa for a cellular network with density between 2 mg/cm^3 and 200 mg/cm^3 [12]) to graphene aerogels obtained by assembly of sol gels at comparable densities. This can be attributed to the hierarchical ordered porosity [14] and in particular to the cellular porosity [12]. The isotropic nature of the architecture contributes to the improved mechanical response. Remarkably, the Young's modulus is even superior to ultralight metallic micro-lattices [44]. Furthermore it is remarkable that for the structures with ordered porosity, the Young's modulus was found to scale with the density (ρ) as $\sim\rho^2$ [58,60] and $\sim\rho^{1.3}$ [12]. The nearly close to linear

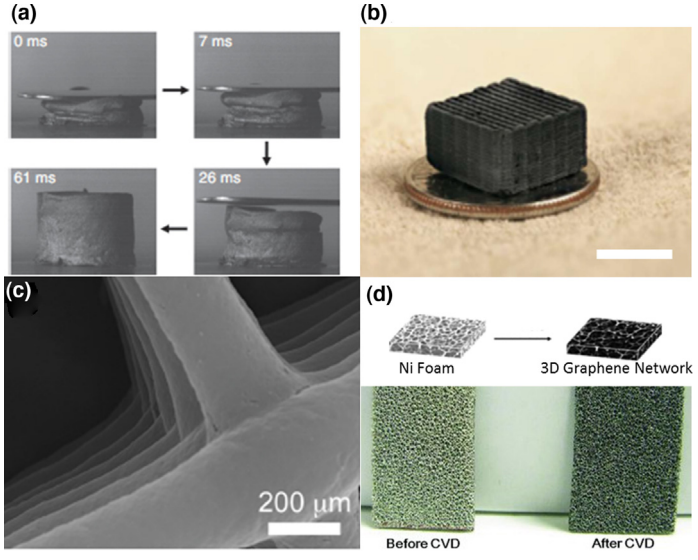

FIGURE 3

(a) Photographs of elastomeric test of CMG networks from freeze-casting (reproduced with permission from [60]); (b) photograph of a 3D CMG monolith produced from 3D printing, scale bar 5 mm (reproduced with permission from [68]); (c) SEM of a 3D printed CMG monolith (reproduced with permission from [67]); and (d) Combined schematic and photograph of CVD graphene growth on commercial nickel foams (adapted with permission from [69]).

Please cite this article in press as: P.C. Sherrell, C. Mattevi, Mater. Today (2016), http://dx.doi.org/10.1016/j.mattod.2015.12.004

dependence of the elastic modulus with the mass density suggests the presence of a hierarchically connected microstructure and possibly even isotropic [14]. Some of these ordered structures have shown extraordinary performances as oil absorbents [7,12,13] and as a joule heating [63] system that arises from the periodic microstructure and sp^2 lattice. Furthermore, cellular structures with a high degree of ordering have also demonstrated reversible superelastic properties exhibited by recoverable shape, and dimensions after 90% compression [12,30,37,60] and after several (up to 1000) cycle of compression they can still recover up to 93% of their original volume [60] (Fig. 3a). This phenomenon often referred to as 'superelasticity' has been found uniquely in grapheme based foams and predominantly in highly ordered graphene networks, while it has not been observed in poorly organized structure with thin walls and small cell sizes [60].

Similarly, templating approaches leveraging hard sacrificial structures, such as polymer bids, ceramic particles [3,62,64,65] or Ni foams [66] have been used to produce CMG network for energy storage applications. While this approach can provide controlled porosity and high specific surface area it is not the method of choice to generate self-supporting monoliths with efficient mechanical properties, since the resulting CMG networks can easily collapse under removal of the sacrificial hard scaffold.

3D printing of self-supporting macro-graphene objects

The most recent development is the achievement of highly ordered and highly controllable free-standing graphene objects in the centimeter size domain range (Fig. 3b) using robotic assisted deposition (3D printing) under ambient conditions [9,67,68]. The macrostructures are formed by a microfilament (Fig. 3c) obtained by a continuous process of extrusion of ink through a nozzle, to form any desirable shape with high precision. A variety of stable periodic 3D architectures have been already demonstrated, such as 'filament piles', 'rings', 'woodpile', '2D geometric hexagonal array', 'open-mesh cylinders', shaped by strands ranging in diameter from 100 μm (Fig. 3c) to 1000 μm [9,67,68].

The most critical parameter for a reliable printing process is the rheology of the inks – requiring non-Newtonian fluid behavior with shear-thinning to allow for flow through nozzles and preservation of the imparted shape. The viscoelasticity properties are also of key importance for the printed struts, as they must be able to sustain the weight of the structure printed on top. Inks based on cross-linked GO [68] or CMG [67], and graphene platelets [9] blended either with viscosifier Silica particles or polymers acting as cross-linker, to reach a shear thinning behavior.

The structures are electrically conductive, mechanically robust, and flexible, and both, electrical conductivity [67,68] (Fig. 2) and Young's modulus [68] can rival graphene aerogels. Overall the elastic modulus is dictated by the microstructure of each filament rather than the geometry of the macrostructure [68]. Electrical conductivity is however similar to CNT sponges (Fig. 2).

Thus the ability to tune the microstructure of the strands is of fundamental importance and research into CMG hydrogels represents the foundation for rational structural design for the mechanical properties.

3D printing of CMG inks is an exciting emerging field with initial printed structures demonstrating great promise for pressure sensors [68] and tissue engineering [9]. The nexus of macroscopic and microstructural control inherent in this process are anticipated to allow graphene objects to be designed to target specific applications with unprecedented levels of control.

Further expansion of inks formulation research via including other 2D materials, such as exfoliated flakes of transition metal dichalcogenides or hexagonal boron nitrides is another promising direction to increase the functionalities of the structures. Additive manufacturing is also a fast developing technology, thus technical advancements are likely to occur in the near future which can greatly expand the printing possibility to nanometric features and scalability of the process.

3D graphene via chemical vapor deposition

Metal foams

The first demonstrations of graphene growth as three-dimensional material arose using commercially available, high purity nickel foams (Fig. 3d) [69,70]. Synthesis of graphene on Ni films has been extensively studied since several decades and it is known to produce few-layered continuous graphene films after exposure to carbon precursors at temperature close to 1000°C. The few-layered growth is driven by the interplay between diffusion-precipitation mechanisms of carbon in bulk nickel at high temperatures. Careful control of the exposure time to carbon precursors and cooling time can lead to tailor the number of layers, from two graphene layers to bulk graphite.

Applying these synthesis principles to highly porous Ni monoliths allowed the growth well connected few-layered graphene architecture [16,17,70–73] with high stiffness and electrical conductivity. The latter is comparable with CVD graphene thin films suggesting that the curvature of the substrate and wrinkling of the graphene do not affect the mechanical properties [69,70]. In addition, five-layered graphene was found to be the optimal thickness to generate the highest electrical conductivity (maximum measured conductivity of 5 S/cm) [70]. The synthesis of graphene is carried out placing the foams in a tubular furnace at low pressure or atmospheric pressure and heated up to temperature comprise between 950 and 1000°C [69,70]. This is then followed by a cooling stage to room temperature. On the contrary to 2D graphene where methane is the most widely used carbon precursors, for 3D networks ethanol [8,74–76], and acetylene [77], are widely used in addition to methane. Ethanol and acetylene are relatively unstable at high temperatures (compared to methane) and are used to induce growth over short time-frames at temperatures lower than 950°C, as required by the high-surface area nanometric metal catalysts used. To finally obtain free-standing 3D graphene foams it is necessary to gently remove the metal scaffold. To this end a methodology already employed to separate graphene films from the Ni planar support, has been implemented and adapted for the 3D foams [70]. This consists of three steps: deposition of polymeric mechanical support, metal etching, and polymer dissolution. The most widely used polymer support is poly(methyl methacrylate) (PMMA), the graphene/Ni foam is normally impregnated in liquid PMMA or the polymer is deposited via immersion/drop casting [69,70] followed by etching of the metal foam in concentrated acids. As the final step PMMA can dissolved in acetone to produce free-standing, 3D graphene foams (Fig. 4a), alternatively a functional polymer can be used for support during metal etching leaving a highly durable flexible

Please cite this article in press as: P.C. Sherrell, C. Mattevi, Mater. Today (2016), http://dx.doi.org/10.1016/j.mattod.2015.12.004

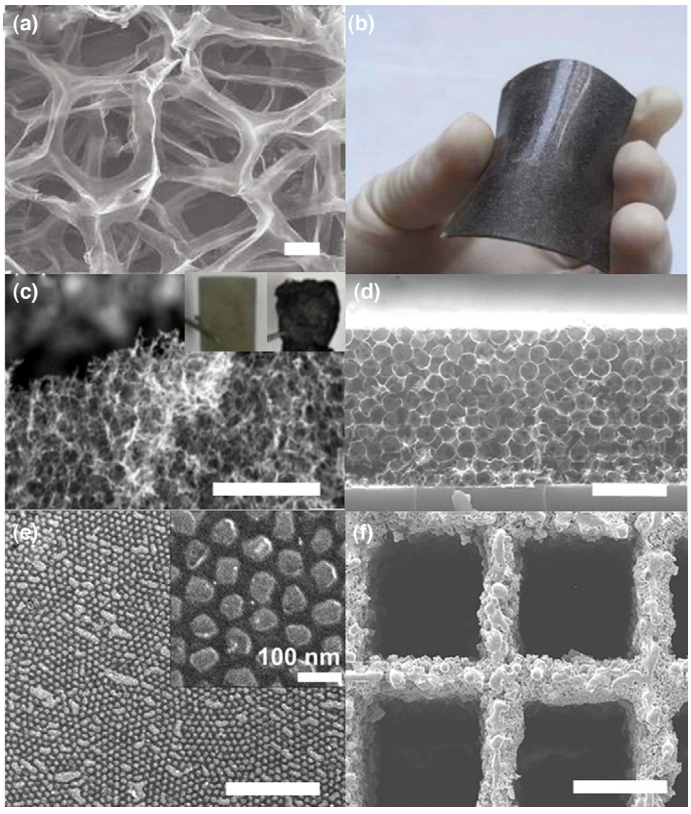

FIGURE 4

Comparison of 3D graphene architectures produced via CVD over various substrate templates: (a) SEM of free-standing 3D graphene synthesized on a commercial nickel foam, scale bar 100 μm (reproduced with permission from [70]); (b) photograph of PMDS, 3D graphene composite for flexible electrode testing (reproduced with permission from [70]); (c) SEM of 3D graphene synthesized from solution processed Ni nanowires scale bar 20 μm (inset photograph of the; left: synthesized graphene monolith on Ni; right: freestanding graphene monolith) (adapted with permission from [90]); (d) SEM of 3D graphene grown from a PVA-Fe precursor via inverse opal templating, scale bar 1 μm (reproduced with permission from [91]); (e) SEM of 3D graphene produced over a AAO templated Au film, scale bar 1 μm (reproduced with permission from [93]); and (f) SEM showing a 3D graphene architecture grown over a 3D printed nickel architecture, scale bar 1 mm (reproduced with permission from [94]).

electrode (Fig. 4b) [70]. Such free standing 3D graphene foams demonstrate excellent electrical conductivity (up to 10 S/cm) at relatively low densities (5 mg/cm^3). The higher conductivities of these foams in comparison to CMG networks (Fig. 2) arise due to the less defected basal plane produced in 3D CVD graphene architectures.

Different nanomaterials such as metal/metal oxide nanoparticles and other 2D materials, can be easily incorporated into the 3D structure to enable additional functionalities to serve different applications. These include: super-capacitors (213–816 F/g) [69,78], flexible electrodes [70,78], strain sensors [79], chemical sensors [74,75], biosensors [8,76,80], and battery electrodes (1155–8700 mA h/g) [81,82]. Graphene 3D networks have been demonstrated also using copper foams as copper is widely used for the synthesis of continuous graphene films for optoelectronic applications as the growth can be self-limited to one layer only. However, graphene 3D networks grown on copper foams have been reported to be mechanically weak and often they do not even present topological continuity to be self-supporting structures, due to the thoroughly single layer graphene films. For this reason, in comparison to nickel, copper foams have not featured prominently within the literature [70].

Comparative to 3D CNT CVD networks, which are either tightly packed aligned CNTs [83] or entangled and highly disordered [84,85], 3D CVD graphene architectures are significantly more anisotropic in terms of electrical conductivity. This difference arises as CNTs via CVD grow perpendicular to the substrate and such networks can be grown either independently of a structured template [84] or via solution coating of a 3D substrate [85]. Due to the high aspect ratio of CNTs 3D CVD architectures are typically only free-standing if produced on a flat substrate with a lateral mechanical support layer (typically a polymer or conductive carbon) [83–86], with architectures produced on 3D templates utilized as synthesized. This provides 3D CVD graphene architectures an inherent advantage over equivalent CNT architectures as they can function as free-standing materials without a heavy, inactive, template impeding device performance. Recent reports have shown great promise by combining the 3D growth of both graphene and CNTs to produce hybrid architectures utilizing the strengths of both materials [87,88].

Advanced structures

The use of commercially available nickel foams as sacrificial template demonstrates the production of mechanically strong and electrically conductive 3D graphene networks. However, there has been minimal studies into the relation between structure and properties of these 3D CVD networks produced on commercial Ni foams, due to the relative homogeneity of available commercial Ni foams.

Therefore to be able to construct graphene scaffolds with controlled structural periodic order bespoke 3D metal catalysts via different metal templating techniques can be used. Approaches offering higher control over pore size and distribution, surface area, and density include: solution processing of metals [6,77,89–91], top-down substrate synthesis [92,93], and additive manufacturing [94]. These various approaches are each attempting to use microstructural control to add device specificity without the requirement of additional functional materials to the produced 3D graphene monoliths.

Solution processing

Nanowire templates from solution

Nickel and copper in the form of nanowires (NWs) with high crystallinity and controlled dimensions can now be studied as CVD graphene templates via solution-based synthesis methods [89,90]. Through stabilization of the nanowires in aqueous media, they could be deposited and assembled through solution processing making them suitable candidates for bottom-up fabrication of scaffolds for graphene constructs.

Copper or nickel NW architectures synthesized through, stamping [89] or vacuum filtration [90], have been demonstrated and employed for 3D CVD graphene synthesis. Low temperatures were required (670°C) to prevent the loss of the micro and nanostructure of the NW template due to melting of the NWs surface. During the heating required for the synthesis of graphene, coherent 3D structures are generated via thermal welding at the intersections

Please cite this article in press as: P.C. Sherrell, C. Mattevi, Mater. Today (2016), http://dx.doi.org/10.1016/j.mattod.2015.12.004

between the NWs [89,90]. Surprisingly, methane was successfully used for such low temperature graphene growth – suggesting the requirement for more reactive carbon species can be overcome even with such delicate metal templates. The welding between the NW templates produced a flexible, interconnected few-layered graphene structure, which has shown promises as strain sensor or flexible electrode with low electrical resistance (Fig. 4c) [89,90]. Control over the final microstructure of NW based 3D graphenes was limited to the size and shape of the produced porosity, obtained by tuning the concentration of the starting NW dispersions.

Polymer templates

The use of polymers as template materials for the growth of graphene allows for gaining significant structural control over graphene architecture. Polymers can be structured at low temperature using a wealth of forming techniques, such as spin coating and inverse opal templating. Subsequently, metals can be deposited [77] or incorporated [6,91] into the polymer and to enable growth of graphene.

Using a tunable block co-polymer blend of polystyrene-poly (ethylene oxide) (PS:PEO) allowed for precise control of pore size through the sacrificial removal of the poly(ethylene oxide). This pore size control arises due to the polymer conformation changes at different PS:PEO ratios, with the removal of the PEO resulting in varying porosity [77]. CVD 3D Graphene was achieved using chemically reduced Ni (as opposed to sputtering/evaporation methods typically required) to coat the porous PS structure, opening pathways for CVD graphene growth on a wide variety of substrates. Similarly to NW templates low temperature CVD was utilized, however, in this case acetylene was used to produce graphene with extremely short growth times [77].

Spin coating of PVA-Ni blends on thermally stable substrates, such as silicon, demonstrated another hybrid solution processing – CVD route to synthesize highly porous 3D graphene structures. For such blended films the PVA decomposition at high temperatures is utilized as a carbon source for graphene synthesis. The obtained thin graphene networks can be removed from substrates using the PMMA transfer method and utilized as a dye-sensitized solar cell electrode [6].

Inverse opal processing techniques, that is, processing using highly regular micro- or nano-beads, have long been used for solution processing synthesis of nanostructures – typically through conductive polymers or carbon loaded polymers. Utilizing a PVA-$FeCl_3$ blend with a silica bead opal template structure allows for CVD growth of 3D graphene in an inverse opal pattern at 1000°C. These highly regular 3D graphene architectures have hierarchical porosity achieved through defects on the individual graphene balls in combination with the large pores from the original silica template (Fig. 4d). Such a hierarchical porosity is suitable for electrochemical applications, in particular super-capacitors, due to the reliance on both rapid ion motion in solution and maximization of the electrochemically available surface area showing exceptional performance as super-capacitor electrodes [91]. Furthermore, such a processing strategy allowed for tuning surface area (448–1025 m^2/g) and conductivity (52–5.4 S/cm) simply by changing the size of the starting silica beads from a diameter of 220–30 nm [91].

Surface modification (top-down)

Top down surface modification provides an excellent route for the control of pore size and distribution over graphene CVD templates. Such top-down methodologies can utilize highly regular pores as in anodic aluminum oxide (AAO) templates [93] or a more random distribution of pore sizes through Kirkendall diffusion during the oxide calcination [92] to produce high surface area templates.

Utilization of a gold-coated AAO as a template for 3D CVD graphene growth allows for precision control over micro-porosity with the resultant self-supporting 3D graphene maintaining the pore size and structure of the starting template (Fig. 4e) [93]. The higher proportion of defects arising from the growth of graphene on gold allows for the introduction of nano-porosity into the AAO templated 3D graphene [93,95].

In contrast to the AAO template which produced extremely regular pore sizes and distribution, a Zn–Mg–Al oxide system utilizing Kirkendall diffusion [92,96] to produce a more random pore structure has been shown to generate high specific surface area templates for direct graphene growth. After CVD graphene growth the oxide templates were removed through NaOH and HCl treatments to produce connected 3D graphene architectures. The produced free-standing graphene architectures had an exceptionally high surface area of 1622 $m^2\ g^{-1}$ due to a distribution of both micro- and meso-pores throughout the structure [92].

Alternatively, high surface area, pseudo-3D nickel templates can be produced by selectively de-alloying manganese from a Ni/Mn alloy [97]. Variations in the alloy composition were shown to roughly tune the pore size of the produced free-standing graphene structures between 100 nm and 2.0 μm allowing for a range of electronic and electrochemical characterization [97].

Additive manufacture

3D printing of metal templates fabrication pathway for device up-scaling into the macro-scale. Selective laser sintering (SLS) enable printing of metals, and functions through focused laser melting of a highly regular metal powder in a layer-by-layer synthesis method producing porosity on the micrometer scale and structural fabrication up to centimeter dimensions. SLS of nickel architectures are a new prospect for 3D graphene growth due to the exceptional structural control afforded by using computer-aided drawing to directly design a growth template [98]. Core limitations of the SLS structures are in the large dimensions (millimeter range) of the smallest features achievable and the roughness of the metal surface. CVD graphene growth requires then long thermal annealing at very high temperature (1370°C for 9 hours) to smooth the Ni surface allowing for graphene growth. The resulting self-supporting 3D graphene architecture had well persevered macro-pore structure of the designed SLS template, demonstrating the first rational design of 3D structure (Fig. 4f) [94].

Remarks and conclusions

We have seen how the fabrication of 3D graphene networks has made significant progress in only five years, from random porosity to controlled hierarchical structures. The approach to fabrication is still dominated by a 'reverse engineering' approach aiming to study the properties of the networks to be then able to build structures with improved mechanical and electrical characteristics by rational design. The aim will be to generate complex structures

Please cite this article in press as: P.C. Sherrell, C. Mattevi, Mater. Today (2016), http://dx.doi.org/10.1016/j.mattod.2015.12.004

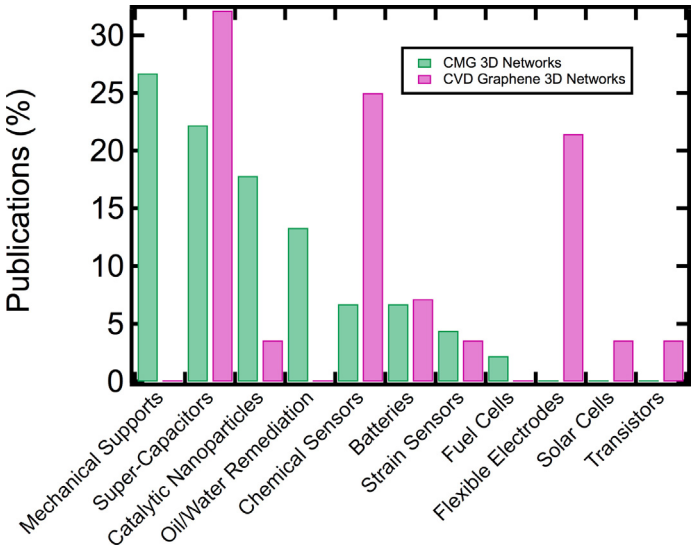

FIGURE 5

Summary of the selected applications studied for CMG monoliths in comparison to 3D CVD graphene monoliths, where electrical properties and specific surface area are crucial, demonstrating a clear focus on flexible electronics, chemical sensors and supercapacitors for CVD graphene networks compared to CMG monolith which are more evenly spread across different technologies with emphasis on sensors and environmental applications (encapsulating oil absorption, water remediation or filtration).

with hierarchical and regular porosity at the micro- and nano-scale. Networks obtained by wet processing are sought primarily for their mechanical properties due to possible easy tunability of elastic response toward application where electrical conductivity is less demanding; comparatively the 3D CVD graphene structures offers superior electrical conductivity which render them more attractive for flexible electronics and as electrodes for electrochemical devices. These tendencies are reflected in the applications for which the structures have been studied and these are summarized in Fig. 5. It is apparent that applications where the most relevant performance is the electrical conductivity are domain of the CVD synthesis while applications where high surface area/density and mechanical properties are critical, wet-processing are employed.

The recent advent of 3D printing of graphene inks in macroscopic objects with microscopic features shows promises for rational design of the microstructures and the knowledge gained by graphene assembly will be of invaluable relevance for designing the properties of the individual filaments holding together the 3D networks. In addition, 3D printing of metal scaffolds as well as graphene inks can largely benefit also from recent progress in ceramic and metals structures using manufacturing techniques that led to demonstration of ultra-light weight complex architectures with remarkable strength.

Moving forward improved understanding of the effect of density, pore-size and shape, and geometry on the electrical and mechanical properties of bespoke 3D CVD graphene architectures, it is anticipated to open up combinational approaches using both CVD and CMG 3D components to fully utilize the exceptional properties of graphene.

Acknowledgements

CM acknowledges the award of a Royal Society University Research Fellowship by the UK Royal Society and the support from the EPSRC through grants EP/K01658X/1, EP/K016792/1. PS would like to acknowledge the funding and support from the European Commission (H2020 – Marie Sklodowska Curie European Fellowship – 660721).

References

[1] K.S. Novoselov, et al. Proc. Natl. Acad. Sci. U. S. A. 102 (30) (2005) 10451.
[2] A.K. Geim, K.S. Novoselov, Nat. Mater. 6 (3) (2007) 183.
[3] B.G. Choi, et al. ACS Nano 6 (5) (2012) 4020.
[4] L. Jiang, et al. Adv. Energy Mater. (2015) 1500771.
[5] C. Hu, et al. Energy Environ. Sci. 8 (1) (2015) 31.
[6] J.-S. Lee, et al. Phys. Chem. Chem. Phys. 14 (22) (2012) 7938.
[7] H. Bi, et al. Adv. Funct. Mater. 22 (21) (2012) 4421.
[8] J. Liu, et al. ACS Appl. Mater. Interfaces 6 (22) (2014) 19997.
[9] A.E. Jakus, et al. ACS Nano 9 (4) (2015) 4636.
[10] P.C. Sherrell, et al. Adv. Funct. Mater. 24 (6) (2014) 769.
[11] E. Murray, et al. RSC Adv. 5 (56) (2015) 45284.
[12] S. Barg, et al. Nat. Commun. 5 (2014) 4328.
[13] H. Sun, et al. Adv. Mater. 25 (18) (2013) 2554.
[14] X. Zheng, et al. Science 344 (6190) (2014) 1373.
[15] Y. Xu, et al. ACS Nano 4 (7) (2010) 4324.
[16] R. Muñoz, C. Gómez-Aleixandre, Chem. Vapor Depos. 19 (10–12) (2013) 297.
[17] Y. Zhang, et al. Acc. Chem. Res. 46 (10) (2013) 2329.
[18] J.M. Wofford, et al. Nano Lett. 10 (12) (2010) 4890.
[19] C. Mattevi, et al. J. Mater. Chem. 21 (10) (2011) 3324.
[20] W. Liu, et al. Carbon 49 (13) (2011) 4122.
[21] B. Hu, et al. Carbon 50 (1) (2012) 57.
[22] D. Geng, et al. Adv. Mater. 27 (18) (2015) 2821.
[23] S. Stankovich, et al. Nature 442 (7100) (2006) 282.
[24] D.A. Dikin, et al. Nature 448 (7152) (2007) 457.
[25] D.R. Dreyer, et al. Chem. Soc. Rev. 39 (1) (2010) 228.
[26] D. Li, et al. Nat. Nano 3 (2) (2008) 101.
[27] G. Eda, M. Chhowalla, Nano Lett. 9 (2) (2009) 814.
[28] G. Eda, et al. Nat. Nano 3 (5) (2008) 270.
[29] W. Gao, et al. Nat. Chem. 1 (5) (2009) 403.
[30] Y. Wu, et al. Nat. Commun. 6 (2015) 6141.
[31] Z. Tang, et al. Angew. Chem. Int. Ed. 49 (27) (2010) 4603.
[32] Q. Tang, et al. Nanoscale 5 (11) (2013) 4541.
[33] W. Chen, L. Yan, Nanoscale 3 (8) (2011) 3132.
[34] H.-P. Cong, et al. ACS Nano 6 (3) (2012) 2693.
[35] H. Bai, et al. J. Phys. Chem. C 115 (13) (2011) 5545.
[36] X. Zhang, et al. J. Mater. Chem. 21 (18) (2011) 6494.
[37] H. Hu, et al. Adv. Mater. 25 (15) (2013) 2219.
[38] H. Bi, et al. Adv. Mater. 24 (37) (2012) 5124.
[39] N.V. Medhekar, et al. ACS Nano 4 (4) (2010) 2300.
[40] Z. Han, et al. Nanoscale 5 (12) (2013) 5462.
[41] Y. Tao, et al. Sci. Rep. 3 (2013) 2975.
[42] M.A. Worsley, et al. Appl. Phys. Lett. 94 (7) (2009) 073115.
[43] K.H. Kim, et al. Adv. Funct. Mater. 23 (3) (2013) 377.
[44] T.A. Schaedler, et al. Science 334 (6058) (2011) 962.
[45] M.A. Worsley, et al. J. Am. Chem. Soc. 132 (40) (2010) 14067.
[46] J. Biener, et al. Adv. Mater. 24 (37) (2012) 5083.
[47] P.M. Sudeep, et al. ACS Nano 7 (8) (2013) 7034.
[48] L.L. Hench, J.K. West, Chem. Rev. 90 (1) (1990) 33.
[49] M.A. Worsley, et al. J. Phys. Chem. Lett. 2 (8) (2011) 921.
[50] Y. Qian, et al. Carbon 68 (2014) 221.
[51] K. Zhang, et al. J. Mater. Chem. 21 (8) (2011) 2663.
[52] S. Vinod, et al. Nat. Commun. 5 (2014) 4541.
[53] M.A. Worsley, et al. ACS Nano 9 (5) (2015) 4698.
[54] S. Deville, et al. Science 311 (5760) (2006) 515.
[55] E. Munch, et al. Science 322 (5907) (2008) 1516.
[56] A. Imhof, D.J. Pine, Chem. Eng. Technol. 21 (8) (1998) 682.
[57] J. Kim, et al. J. Am. Chem. Soc. 132 (23) (2010) 8180.
[58] N. Ni, et al. Sci. Rep. 5 (2015) 13712.
[59] L. Estevez, et al. J. Am. Chem. Soc. 133 (16) (2011) 6122.
[60] L. Qiu, et al. Nat. Commun. 3 (2012) 1241.
[61] X. Xie, et al. Sci. Rep. 3 (2013) 2117.
[62] J.L. Vickery, et al. Adv. Mater. 21 (21) (2009) 2180.
[63] R. Menzel, et al. Adv. Funct. Mater. 25 (1) (2015) 28.
[64] C.-M. Chen, et al. Chem. Commun. 48 (57) (2012) 7149.
[65] X. Huang, et al. Adv. Mater. 24 (32) (2012) 4419.

Please cite this article in press as: P.C. Sherrell, C. Mattevi, Mater. Today (2016), http://dx.doi.org/10.1016/j.mattod.2015.12.004

[66] Z.Y. Xia, et al. Carbon 84 (2015) 254.
[67] E. García-Tuñon, et al. Adv. Mater. 27 (10) (2015) 1688.
[68] C. Zhu, et al. Nat. Commun. 6 (2015) 6962.
[69] X. Cao, et al. Small 7 (22) (2011) 3163.
[70] Z. Chen, et al. Nat. Mater. 10 (6) (2011) 424.
[71] A. Reina, et al. Nano Lett. 9 (1) (2009) 30.
[72] X. Li, et al. Nano Lett. 9 (12) (2009) 4268.
[73] Y. Zhang, et al. J. Phys. Chem. Lett. 1 (20) (2010) 3101.
[74] X. Dong, et al. J. Mater. Chem. 22 (33) (2012) 17044.
[75] F. Xi, et al. Electrochem. Commun. 26 (2013) 81.
[76] J. Liu, et al. Electrochim. Acta 161 (2015) 17.
[77] K. Liu, et al. ACS Nano 9 (6) (2015) 6041.
[78] J. Zhi, et al. Adv. Funct. Mater. 24 (14) (2014) 2013.
[79] Y.R. Jeong, et al. Adv. Funct. Mater. 25 (27) (2015) 4228.
[80] Y. Ma, et al. Biosens. Bioelectron. 59 (2014) 384.
[81] B. Wang, et al. J. Mater. Chem. A 3 (26) (2015) 13691.
[82] X. Guo, et al. Adv. Mater. 27 (40) (2015) 6137.
[83] Z.F. Ren, et al. Science 282 (5391) (1998) 1105.
[84] J. Chen, et al. Adv. Mater. 20 (3) (2008) 566.
[85] J. Chen, et al. Energy Environ. Sci. 2 (4) (2009) 393.
[86] L. Ci, et al. Adv. Mater. 19 (20) (2007) 3300.
[87] Y. Xue, et al. Sci. Adv. 1 (8) (2015).
[88] W. Zhang, et al. Carbon 86 (2015) 358.
[89] H. Xu, et al. Nanoscale 7 (24) (2015) 10613.
[90] B.H. Min, et al. Carbon 80 (2014) 446.
[91] J.-C. Yoon, et al. Sci. Rep. 3 (2013) 1788.
[92] J.-L. Shi, et al. Small 11 (39) (2015) 5243.
[93] I. Jung, et al. Appl. Phys. Lett. 103 (2) (2013) 023105.
[94] Z. Yang, et al. RSC Adv. 5 (37) (2015) 29397.
[95] T. Oznuluer, et al. Appl. Phys. Lett. 98 (18) (2011) 183101.
[96] R.W. Balluffi, L.L. Seigle, Acta Metall. 5 (8) (1957) 449.
[97] Y. Ito, et al. Angew. Chem. Int. Ed. 53 (19) (2014) 4822.
[98] C. Zhao, et al. Electrochem. Commun. 41 (0) (2014) 20.

Please cite this article in press as: P.C. Sherrell, C. Mattevi, Mater. Today (2016), http://dx.doi.org/10.1016/j.mattod.2015.12.004